Charles University in Prague

Faculty of Mathematics and Physics

**BACHELOR THESIS**

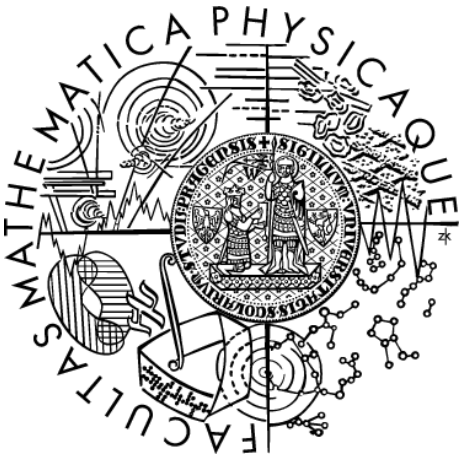


Radek Podškubka

# Analýza dlouhodobého vývoje jasu noční oblohy na Observatoři Pierre Augera

# The night sky brightness at the Pierre Auger Observatory and its long-term correlation with the solar activity

The Astronomical Institute of Charles University in Prague

Supervisor of the bachelor thesis: RNDr. Michael Prouza, Ph.D.

Study programme: Physics

Specialization: Nuclear and subnuclear physics

Prague 2012

I am grateful to my supervisor, Michael Prouza. His support was priceless. The completion of this thesis would be impossible without his guidance. Besides I would like to thank to my parents for their moral help.

I declare that I carried out this bachelor thesis independently, and only with the cited sources, literature and other professional sources.

I understand that my work relates to the rights and obligations under the Act No. 121/2000 Coll., the Copyright Act, as amended, in particular the fact that the Charles University in Prague has the right to conclude a license agreement on the use of this work as a school work pursuant to Section 60 paragraph 1 of the Copyright Act.

In Prague 21.5.2012 signature of the author

Název práce: Analýza dlouhodobého vývoje jasu noční oblohy na Observatoři Pierre Augera

Autor: Radek Podškubka

Katedra: Astronomický ústav Univerzity Karlovy v Praze

Vedoucí bakalářské práce: RNDr. Michael Prouza, Ph.D., Fyzikální ústav AV ČR, v. v. i.

Abstrakt: V této práci srovnáváme jas noční oblohy v oblasti observatoře Pierra Augera s tokem extrémního UV záření ze Slunce. Jas noční oblohy je měřen během aktivní činnosti fluorescenčních detektorů. Data byla zpracována několikrát různými postupy tak, aby byl vyloučen vliv měsíčního svitu, světelného znečištění a oblačnosti. V případě, že neuvažujeme tyto efekty, je hlavním zdrojem jasu noční oblohy airglow. Cílem je ukázat, že jas noční oblohy koreluje s tokem extrémního UV záření, což by potvrdilo, že extrémní UV záření je hlavní příčinou vzniku airglow.

Klíčová slova: airglow, sluneční aktivita, jas noční oblohy

Title: The night sky brightness at the Pierre Auger Observatory and it's long-term correlation with the solar activity

Author: Radek Podškubka

Department: The Astronomical Institute of Charles University in Prague

Supervisor: RNDr. Michael Prouza, Ph.D., Institute of Physics ASCR, v. v. i.

Abstract: In this paper we compare night sky brightness at the Pierre Auger Observatory with the flux of the solar extreme UV radiation. The night sky brightness is measured for monitoring purposes during operation of fluorescence detectors. The data were processed several times under slightly different conditions that should exclude the impact of moonlight, artificial light pollution and cloudiness. If one does not consider the effects mentioned before, the main source of night sky brightness is an airglow. The goal is to show that night sky brightness correlates with the flux of solar extreme UV radiation, what will confirm that extreme UV radiation is the cause of the airglow origin.

Keywords: airglow, solar activity, night sky brightness

# Contents

# Introduction

Pierre Auger Observatory is the largest observatory that performs research in the field of astroparticle physics. The main purpose of this observatory is to investigate cosmic ray particles with the highest energies, chemical composition of cosmic rays, arrival direction of these particles and investigation of accelerating mechanisms that are able to accelerate cosmic ray particles up to such high energies.

Pierre Auger Observatory is so called hybrid detector. It means that there are both surface detectors and fluorescence detectors. Fluorescence detectors monitor also night sky brightness during the time of their operation. These data are very useful for the monitoring of night sky brightness variability.

The main goal of this paper is to investigate relation between solar cycle and night sky brightness variation on long time scales. There are many effects that contribute by different measure to night sky brightness. Since our goal is to show correlation between solar cycle and night sky brightness it is necessary to exclude sources of night sky brightness that has certainly no relation to solar cycle. After this correction it is possible to inspect any correlation. If we exclude the effects that have no connection to solar activity we may claim that the major source of night sky brightness is an airglow effect.

This type of analysis has never been performed using the backround data from fluorescence detectors.

# 1. Theory

## 1.1 Cosmic ray spectrum

We define cosmic rays as interstellar particles that reach the Earth atmosphere. Considering the chemical composition, protons, hydrogen and helium nuclei dominate at the GeV energies. However, we believe that cosmic rays consist of all stable nuclei, although the occurrence of other nuclei could be very rare. Photons and neutrinos may also be primary cosmic ray.

We will start with the energy spectrum of cosmic rays. The energy range of cosmic rays is very wide. The most important is the interval of energies from 100 GeV per nucleus and higher. This is the total energy of the primary particle. Furthermore, in the region of such a high energy levels, the kinetic energy of light nucleus (for example hydrogen nucleus with invariant mass $m_p = 0.938$ GeV) is approximately equal to the total energy. This statement, however, is not true for lower kinetic energies.

The energy spectrum is defined as the dependence of the cosmic ray flux on the energy. It is natural that energy spectrum shows the decrease of cosmic ray flux with higher energies. For example the value 6 particles per square kilometer per minute is flux that is relevant to the energy of $10^7$ GeV. The flux for higher energies is much lower. It decreases by a factor of $10^{-3}$ per decade of energy. It is

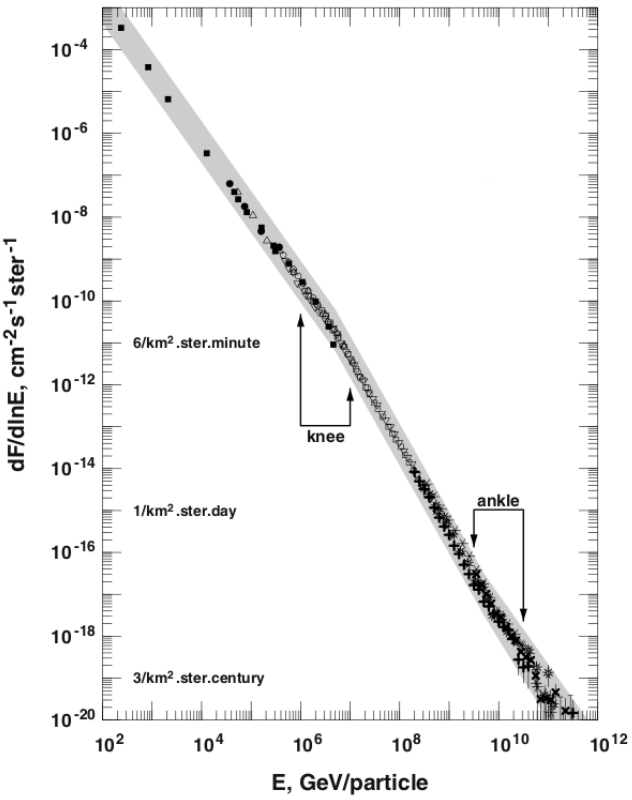


Figure 1.1: Cosmic rays energy spectrum. This figure is taken from [4].

the major difficulty that contemporary projects has to face. The graphical representation of cosmic ray energy spectrum is at the Figure 1.1. If we carefully look

at this figure, we find out that there are two regions, where cosmic ray spectrum clearly changes its slope. At first it become steeper between $10^6$ and $10^7$ GeV. This region is called "knee".

Between $10^9$ and $10^{10}$ GeV spectrum becomes again flatter. This region is called "ankle". We still not understand this region very well. However, we believe that the existence of "knee" in cosmic ray spectrum is the consequence of different accelerating processes of cosmic rays with energies above and below the knee. The "ankle" is considered as the border. Cosmic rays with energies higher then the energy of "ankle" are considered as a cosmic rays of extragalactic origin.

It is necessary to emphasize that Large Hadron Collider can reach energies around $10^4$ GeV. If we want to examine particles accelerated to higher energies, it is necessary to investigate cosmic rays because it is contemporary the only source of particles with such a high energies.

## 1.2 Cosmic ray showers

Cosmic ray shower is the cascade of particles initialized by some primary particle which interacts in the upper atmosphere. This cascade is quickly developing and very complex. It consists of electromagnetic and hadronic components. The flux of high energy primary particles is very low. Therefore the analysis of cosmic ray showers is the only way to learn about such energetic primary particles.

The basic idea of cosmic ray shower development is illustrated by Heitler's toy model [4]. According to this model the depth of the maximum of the shower, that is denoted $X_{max}$ is proportional to the logarithm of primary particle energy. We assume that the cascade is made of the particles of the same type. The particle interacts after the length $\lambda$ while creating two new particles each carrying half of the energy of former particle. After $n$ interactions at the depth $n\lambda$, cosmic ray shower consists of $2^n$ particles each carrying the energy $E = \frac{E_0}{2^n}$. As the energy of the particle is decreasing, the cross-section of the interaction is decreasing too. When the particle reaches critical energy $E_C$ the interaction cross-section is zero and particles will interact no more. The maximum possible number of particles is $N_{max} = \frac{E_0}{E_C}$. So the $X_{max}$ is defined according the formula (1.1)

$$X_{max} = \lambda \log_2 N_{max} = \lambda \log_2 \left( \frac{E_0}{E_C} \right) \tag{1.1}$$

Even though the Heitler's model is very simple it describes sufficiently the basic properties and propagation of electromagnetic component of cosmic ray air shower as well as the hadronic component. It was shown that according to this model the depth of the maximum $X_{max}$ is proportional to the logarithm of primary particle energy as was suggested at the beginning of this Section.

## 1.3 Cosmic ray detectors

As we mentioned above, the detection of secondary cosmic ray shower is essential to learn about the properties of primary particle. There are plenty of detection techniques and many detector types, which are useful in various applications in

particle physics. Even though there is many detection techniques, in astroparticle physics there are only few detector types which are commonly used. As a surface detector Cherenkov or scintillation detectors are used and for atmosphere monitoring only fluorescence detection technique is used. We will describe detectors that are used at the Pierre Auger Observatory. These are the fluorescence detectors and the Cherenkov surface detectors. Fluorescence detectors will be emphasized much more, because the data analyzed in this paper are collected by fluorescence detectors.

## 1.4 Pierre Auger Observatory

The Pierre Auger Observatory is studying high energy cosmic rays, these cosmic rays reach energies up to $10^{20}$ eV. The main purpose of the Pierre Auger Observatory is to learn about the origin of cosmic rays and to study properties of these rare particles. Particles with the highest energies (energies around $10^{20}$ eV) hit the atmosphere of Earth very seldom, approximately 1 particle per km$^2$ per century. If one wants to do quality research it is necessary to collect a large volume of data. Therefore surface of the observatory is very large. Pierre Auger Observatory area covers 3000 km$^2$ of pampas in Mendoza province in Argentina. It is the largest high energy cosmic ray detector in the world.

This observatory is so-called hybrid cosmic ray observatory. It combines measurements performed by surface Cherenkov detectors and also by UV sensitive fluorescence detectors (FDs). There are 24 FDs, which monitor the area of the observatory. There are also 1600 Cherenkov water detectors, which are regularly distributed over the area of the observatory in a hexagonal grid. The map of Pierre Auger Observatory is at the Figure 1.2.

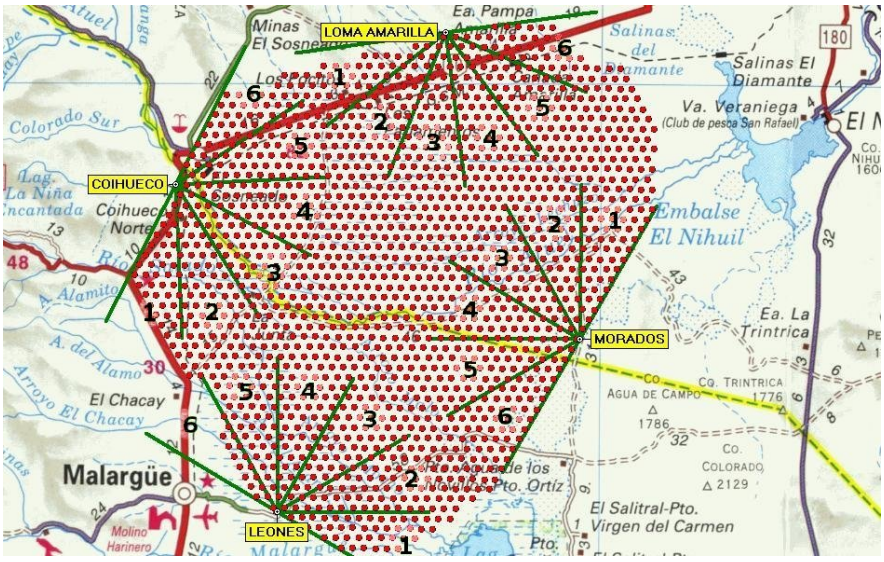


Figure 1.2: Map of Pierre Auger Observatory. Red dots denote surface detectors and green lines delimit the field of view of every single bay of fluorescence detector. Black numbers correspond to the number of FD camera.

When the primary particle of cosmic ray hits the Earth's atmosphere it produces the shower of secondary particles. Some of these secondary particles reach

the ground and they are detected by Cherenkov water detectors. As the shower propagates in the atmosphere it might excite nitrogen atoms. Nitrogen atoms recombine and they emit UV radiation which is measured by FDs.

## 1.5 Surface detectors

Surface detector array consists of 1600 Cherenkov detector stations covering the area of 3000 km$^2$. As the name of the detector suggests it works on the principle of detecting the Cherenkov radiation, which originates as a product of Cherenkov effect [5].

### 1.5.1 Cherenkov light

Cherenkov radiation is an electromagnetic radiation. It originates when some charged particle travels through dielectric material with speed exceeding the phase velocity of light in that material. According to the special theory of relativity, the speed of light in the vacuum, is the limit velocity. We denote this speed as $c$. However, the speed of light in materials could be significantly lower than $c$ (for example, the speed of light in water is $0.75c$). If particle moves in any material faster than phase velocity of light in that medium, it is not in contradiction with Einstein's special theory of relativity.

Let us suppose that such a charged particle moves through the dielectric medium. It disrupts electromagnetic field in the material and polarizes atoms of that medium. Photons are emitted as electrons return to their original state. In normal case these photons would destructively interfere with each other. However when disruption is faster than the velocity of light in that medium, photons interfere constructively and the light is observable.

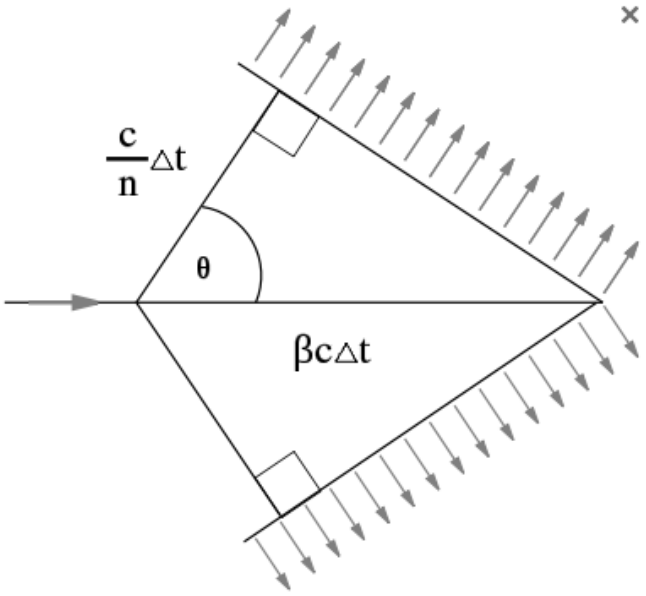


Figure 1.3: Scheme of Cherenkov light emission. This scheme is taken from [4].

Furthermore let us suppose that the speed of the charged particle is $v_e$ and it meets the relation $\frac{c}{n} < v_e < c$, where $n$ is refractive index of relevant material. As

the particle propagates in the medium, the photons are emitted. The radiation is observed only under the angle $\theta$ with respect to the path of the particle. This angle represents the direction in which the photons are coherent and combine a planar wave. Within the time interval $\Delta t$ (since the entry of the particle to the material $t = 0$) the particle travels the distance $x_e = v_e \Delta t = \beta c \Delta t$, while the photons emitted in the time $t = 0$ reach the distance $x_p = \frac{c}{n} \Delta t$ from the place of their origin. We still assume that the radiation propagates as a planar wave so from the trigonometry it is clear that the angle $\theta$ meets the condition (1.2). The geometry is drown at the Figure 1.3.

$$\cos(\theta) = \frac{1}{n\beta} \tag{1.2}$$

### 1.5.2 Detector design

Each detector has the shape of circular tank with 3.5 m diameter. It contains 12 000 l of clear water, where Cherenkov light originates. Photons are detected by 3 photomultipliers which looks down to the water.

The water Cherenkov detectors were chosen because of their low cost and their sensitivity to charged particles as well as to energetic photons that convert to pairs in the water [5]. Moreover, the surface array has almost 100% duty factor. On the other hand, the surface detectors are only able to sample shower at the groud level. Therefore we are not able to determine directly the energy of primary particle. If one has only the data from surface Cherenkov detectors, it is necessary to use some interaction models to get the energy of primary particle.

## 1.6 Fluorescence detectors

### 1.6.1 Air fluorescence

As we have described above, when primary particle interacts in the upper part of the atmosphere, it starts the shower of secondary particles. The longitudinal profile of the shower is detected by fluorescence telescopes. The energy of primary particle is reconstructed. Some fraction of the energy of primary particle is carried away by neutrinos and because the energy deposit of muons is very small. This fraction of energy is so called missing energy. Fortunately some correction exists and it is possible to measure the energy of primary particle with relatively well precision.

The fluorescence detection techniques take advantage of the excitation or ionization of nitrogen molecules by secondary particles of cosmic ray shower. The nitrogen molecules which are in higher energy states deexcite and emit photon in UV region. This radiation is also called fluorescence light. The fluorescence light is produced isotropically. Thanks to this fact fluorescence detectors are able to look for air showers developing high above the ground and inspect their longitudinal profile.

According to [6] it is assumed that number of emitted fluorescence photons is proportional to the energy deposited in the atmosphere. Denoting $dN_\gamma$ the number of fluorescence photons emitted per the atmosphere volume of thickness

$dX$, we could derive the relation (1.3)

$$\frac{dN_\gamma}{dX} = \frac{dE_{dep}^{tot}}{dX} \int Y\left(\lambda, p, T, u\right) \tau\left(\lambda, X\right) \varepsilon\left(\lambda\right) \, \mathrm{d}\lambda \tag{1.3}$$

$\tau$ denotes the transmission of the atmosphere and $\varepsilon$ is the efficiency of fluorescence detector. Fluorescence yield $Y$ describes the number of emitted photons per deposited energy. We suppose that $Y$ does not depend on the energy of secondary particle. The relation (1.3) describes very well that the number of emitted photons is proportional to the total energy deposited in the atmosphere. However, while the air shower is developing in the atmosphere it does not produce only fluorescence light. The Cherenkov effect contributes too. Cherenkov light is observable mostly in the direction of the shower axis so this effect has to be eliminated by some correction which depends on the mutual geometry of shower and fluorescence detector.

### 1.6.2 Design of the fluorescence detectors

At Auger observatory the fluorescence light is detected by 4 FD stations. Each of these stations contains 6 fluorescence telescopes with a spherical mirror, filter that selects light in wavelength range 300 - 410 nm and refractive correction ring. These rings were not installed at the same time. The dates of installation of correction rings are in the Table 6.1 in the Attachments. The significant component of detector is an array of 440 photomultiplier tubes in the focal plane of the mirror. Spatial resolution of each mirror is 30° (azimuth) × 28° (elevation). It means that the field of view of each fluorescence detector is 180° in azimuth.

The signal from FD is regarded as cosmic ray shower only if it pass through a three - stage trigger system [8].

The first level of the trigger system selects only the events on the basis of the number of triggered pixels. This level is naturally called channel threshold. The second level selects only the events with linear shape of triggered pixels because the track of the cosmic ray shower tends to be linear. The picture of patterns regarded as straight tracks is at the Figure 1.4.

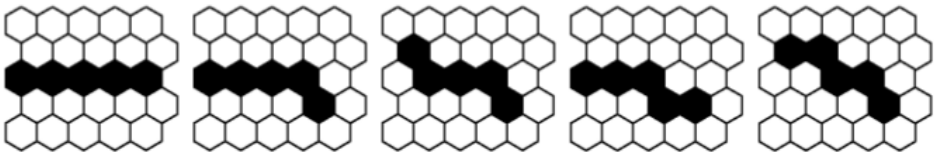

Figure 1.4: Basic types of patterns regarded as straight track. This picture is taken from [8].

The second level is called track shape trigger. Third level of trigger system is so called lighting rejection trigger. This trigger is designed to exclude pixels triggered randomly or triggered by lightning.

The main goal of the FD is to reconstruct cosmic ray shower profile and its trajectory. At first it is necessary to find out the position of the shower. The position could be denoted by the impact parameter $R_T$. Impact parameter is the

shortest distance from shower trajectory to the detector. The trajectory reconstruction of the shower is quite straightforward, if there are two or more FDs that detected the shower. Each triggered FD determines the plane where the trajectory of the shower lies. The trajectory matches the line of intersection of these planes. If only one FD is triggered the determination of exact trajectory could be more troublesome but it is possible in principle. One can use time differences between the responses of neighboring phototubes. It is obvious that nearby showers are faster than distant showers. This is the key fact which is used in further reconstruction.

Charged particle in the shower excites nitrogen in the atmosphere. According [4] there is a rough estimate that one electron creates four photons per one meter, but the exact number of created photons depends on the atmospheric conditions. However fluorescence light is absorbed in the atmosphere. Absorption depends strongly on the atmospheric conditions so it is necessary to monitor the atmosphere in order to perform proper corrections.

Final step is to determine energy of primary particle. As we mentioned at the beginning of this section, some fraction of primary particle energy is transfered to non-interacting neutrinos. This energy is called missing energy.

### 1.6.3 Background measurements

FDs are primarily used for cosmic ray measurements, but they monitor also background brightness of the night sky. The background measurements could be used for better understanding of night sky brightness variation and processes possibly connected to these variations. Although photomultipliers' output is not directly value of photon flux, it is possible to get information about sky brightness from the photomultipliers' measurements of signal variances which are proportional to the photon flux.

Variance of the signal is sampled each 100 ns and from 65535 samples the average is determined. This value is measured each 30 s [10]. The main purpose of such a measurements is to monitor background brightness to save life time of photomultipliers.

## 1.7 Night sky brightness sources

There are lots of light sources contributing to the moonless night sky brightness both terrestrial and non-terrestrial. According to [1] non-terrestrial light sources contribute to the night sky brightness to a lesser extent than terrestrial light sources. The most significant light sources are airglow 60%, zodiacal light 27%, light scattered by interstellar dust 5% and integrated brightness of faint unresolved stars 2%.

The airglow is the major component of the night sky brightness. It has origin in Earth's atmosphere at an altitude about 100 km. Airglow is emitted by molecules and atoms which are excited by solar EUV radiation during the day. Its spectrum includes OI spectral lines both 557,7 nm and 630 nm, also NaD doublet 589 nm and OH rotational and vibrational bands [1]. In the airglow spectra there is quite distinct green continuum and faint blue continuum.

The most noticeable is OI spectral line 557,7 nm that causes green color of

airglow. Nevertheless, $O_2$ Herzberg bands between 250 nm and 490 nm are the most important for us, because this wavelength range spans over the range of sensitivity of FD telescopes. Thanks to this fact it is possible to examine FDs' background measurements and find out how much Herzberg bands emissions affect night sky brightness. Comparing these data with solar EUV radiation we can determine the correlation between airglow intensity and solar activity. The airglow spectrum is at the Figure 1.5.

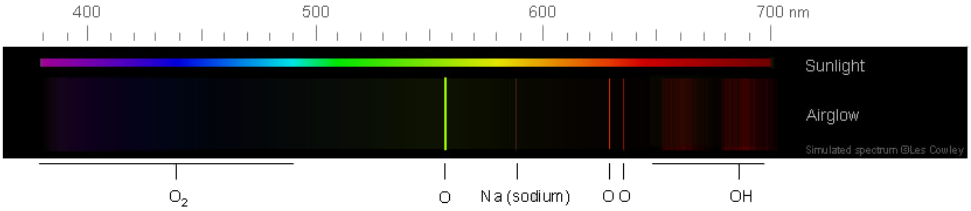


Figure 1.5: Airglow spectrum in the wavelength range of visible light.

### 1.7.1 The near UV and blue spectrum of airglow

Investigation of the blue and UV spectrum of airglow is quite exacting because in this wavelength region many of bands are overlapping. In fifties it was first suggested that forbidden Herzberg bands contributes significantly to the blue and near UV component of airglow.

The main source is forbidden Herzberg I band system $A^3\sum_u^+ \longrightarrow X^3\sum_g^-$. This emission is consequence of recombination of oxygen atoms which are remnant of daytime photo-dissociation of oxygen molecules. It is broadly believed that the reaction (1.4), which takes place in the upper atmosphere (around 100 km), is the main contributor to the Herzberg I band [7].

$$\mathrm{O} + \mathrm{O} + \mathrm{M} \longrightarrow \mathrm{O}_2\left(A^3\sum_u^+\right) + \mathrm{M} \tag{1.4}$$

According [7] it may be possible that reaction (1.5) also contributes to the airglow Herzberg I band.

$$\mathrm{N} + \mathrm{O}_3 \longrightarrow \mathrm{O}_2\left(A^3\sum_u^+\right) + \mathrm{NO} \tag{1.5}$$

This reaction takes place around 80 km height. Naturally there is a maximum of the intensity of Herzberg I band system during the night because the dissociation of molecules does not occur at night and the number of atomic oxygen and nitrogen decreases due to the recombination.

Due to the relatively complex structure of near UV and blue part airglow spectrum, it is not possible to state that Herzberg I band is the only contributor. However it is the only fully confirmed source. The presence of other proposed sources is still not fully established [7].

## 1.8 Extreme ultraviolet radiation

Extreme ultraviolet radiation is electromagnetic radiation with wavelengths from 120 nm to 10 nm with corresponding energies (according to Planck's law) from

10 eV to 124 eV. Natural source of EUV radiation is solar corona. EUV requires very high vacuum for its propagation so it is absorbed in the Earth's atmosphere.

EUV radiation is emitted while an electron is bounding to some positive multicharged ion. Such ions could be found in hot plasma of solar corona so it is an ideal natural source of EUV radiation.

## 1.9 Solar cycle

Solar cycle is a periodic change in a solar activity. The amount of solar radiation coming to the Earth is related to solar activity. Intensity of solar EUV flux periodically changes with solar cycle that is about 11 years long. Of course there are some minor fluctuations which are not related to the solar cycle. The variations of the solar activity are apparent also in the varying number of sunspots in the solar photosphere. The number of sunspots is a useful quantity, which is commonly used to express the intensity of solar activity.

The solar activity might be quantified e.g. using the Wolf number, which is calculated using the exact number of sunspots and groups of sunspots during the day. This quantity is defined according the formula (1.6)

$$R = k\,(10g + s) \tag{1.6}$$

Where $g$ is a number of sunspot groups, $s$ is a number of individual sunspots and $k$ is an observatory factor, which varies with the location on the Earth and with an instrument, which is used for the observation.

As one can see at the Figure 1.6, the last solar minimum was observed in 2009 and the last solar maximum was in 2002.

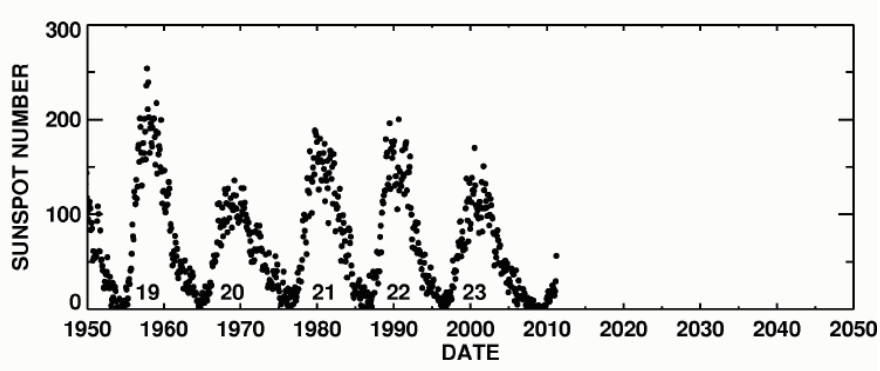


Figure 1.6: Wolf number time development by NASA/MSFC.

Other possibility how to determine the intensity of solar activity is solar EUV flux measurement. These measurements are performed for example by solar EUV monitor (SEM) on SOHO spacecraft. As one can see at the Figure 1.7, the solar cycle maximum is well observable.

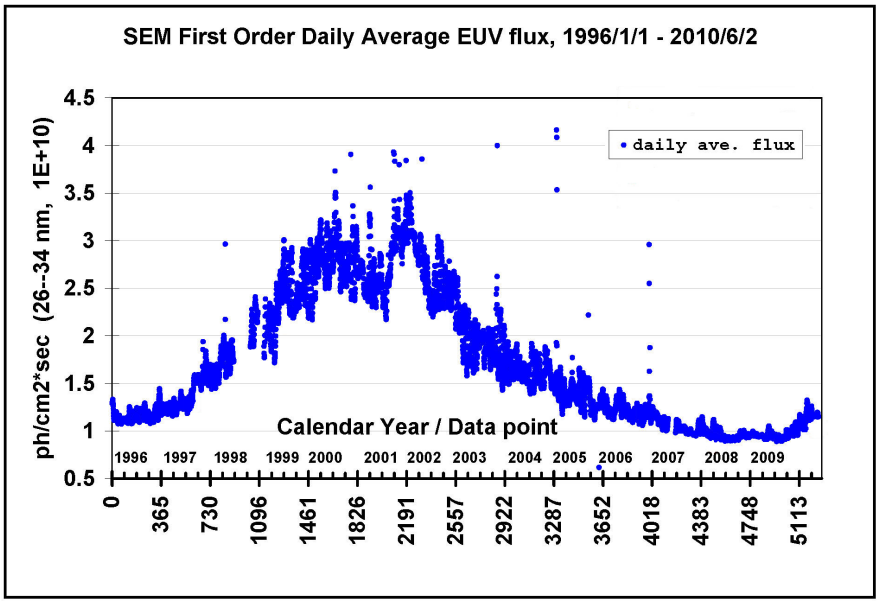


Figure 1.7: Solar EUV flux measured by SOHO spacecraft.

# 2. Time variations

Night sky brightness varies very rapidly with time. This variation is observable both on short time scales as well as on long time scales. As it was suggested in Chapter 1, our goal is to determine correlation between the night sky brightness and the solar EUV radiation flux. In this work, we have focused on the longer time scales, and thus on the comparison with the 11-year cycle of the solar activity. We have analyzed the background data since August 2004 until October 2010. The results of this long-term analysis are discussed in the next sections.

Quite naturally, the background brightness of the sky is also greatly affected by other sources of light. The most significant natural source is certainly Moon. If we focus on the night from January 4, 2008 to January 5, 2008, when Moon rose at 2:00 a.m., we notice that around 2:00 a.m. variances grew rapidly. Background brightness development of this night is at the Figure 2.1.

Except Moon there are some other effects that can also influence background brightness. It is possible that cloudiness, human light pollution or Milky Way affect background brightness variability. Of course we can avoid the influence of these parasitic effects by exclusion of affected data. On the other hand we have to maintain sufficient volume of data to keep good statistics.

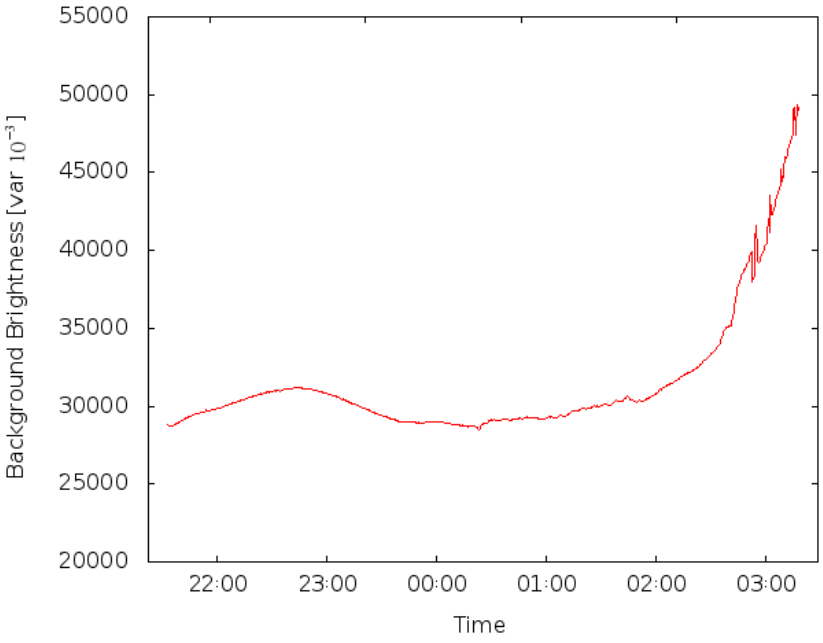


Figure 2.1: Development of background brightness at Los Leones bay 1 during the night from January 4, 2008 to January 5, 2008.

## 2.1 Datasets preparation

All data affected by moonlight are excluded. Only measurements where variances are higher then 10 and lower than 100 are accepted. The lower bound ensures that measurements with closed shutters are excluded and the upper bound ensures

that measurements influenced by electronic error are excluded.

Daily median is calculated using such a filtered data. We accept only the days when more than 400 measurements were used for calculating the daily median. Then monthly average is made. If there are less then 5 days available in one month we leave that month out.

## 2.2 Datasets comparison

The outcome of the process described above is compared with solar EUV radiation measured by Solar EUV monitor (SEM) on SOHO spacecraft [3]. These data are publicly available. SEM is sensitive in wavelength range from 0.1 nm to 50 nm. SEM measurements are well calibrated so the available data correspond to the values of solar EUV flux at a distance of 1 AU from the Sun. The goal is to show that these data correlate with the background brightness. The extent of agreement between two datasets can be expressed by Pearson correlation coefficient.

### 2.2.1 Pearson correlation coefficient

Pearson correlation coefficient expresses the strength of a linear dependence between two variables [9]. These two variables are intensity of the signal from photomultiplier and solar EUV radiance flux. Pearson correlation coefficient (commonly denoted $r$) is defined according to the formula (2.1).

$$r = \frac{\sum_{i=1}^{n} \left(X_i - \overline{X}\right)\left(Y_i - \overline{Y}\right)}{\sqrt{\sum_{i=1}^{n} \left(X_i - \overline{X}\right)} \sqrt{\sum_{i=1}^{n} \left(Y_i - \overline{Y}\right)}} \tag{2.1}$$

Where $X_i$ and $Y_i$ are every single values. The values $\overline{X}$ and $\overline{Y}$ are arithmetical means of all measurements. Coefficient $r$ ranges from $-1$ to 1. Positive values of $r$ mean that datasets correlate while negative values of $r$ mean anticorrelation. Naturally the higher is the value of $r$ the better is the correlation between two datasets. Although there is no exact and general interpretation of Pearson correlation coefficient, because such interpretation depends on the circumstances and context of the problem, some authors offer guidelines for the interpretation of a correlation coefficient [11]. This interpretation is in the Table 2.1. According to this guideline, it is possible to claim that if $r$ is higher than 0.5, then the correlation is significant.

| **Correlation** | **Coefficient** |
|---|---|
| None | 0.0 to 0.09 |
| Small | 0.1 to 0.3 |
| Medium | 0.3 to 0.5 |
| Strong | 0.5 to 1.0 |

Table 2.1: Interpretation of the Pearson correlation coefficient according to [11].

## 2.3 Analysis of the signal using the full area of FD camera

Data from FD stations Los Leones, Coihueco and Los Morados were analyzed. Each FD station contains 6 so called bays with one FD telescope. Signal from all PMTs of each FD telescope is included. Concerning Loma Amarilla FD station, there is a lack of data because this FD station started its operation later. Thus the statistics is very poor, and it was not analyzed in this work.

Considering Coihueco FD station, the best correlation between background brightness and solar EUV radiation was achieved in case of bay 4. The field of view of this bay is not affected by human light pollution or by turbulent atmospheric conditions above Andas. Pearson correlation coefficient is equal to $r = 0.63$. One can regard this as a good correlation. At the Figure 2.2 there is a graph showing time development of background brightness measured by bay 4 and there is also time development of solar EUV flux. On one hand it is evident that the trend of both datasets is the same. There are also agreements in some local extremes, for instance in the end of 2006. On the other hand there is a strong deviation of background brightness variance around May 2008 and April 2010. It is apparent that these deviations were also measured in different extents by other FDs. Pearson coefficients and figures with graphs related to the other bays are in Attachments.

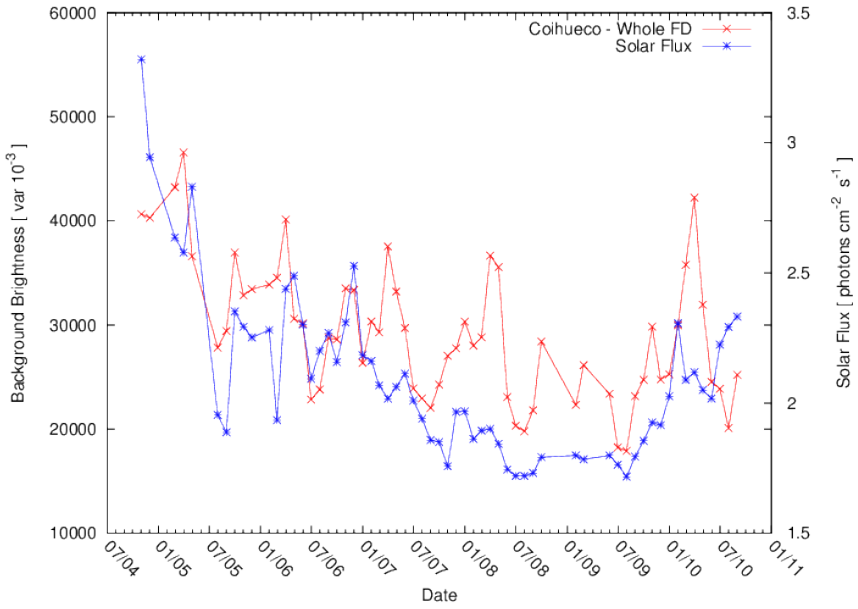


Figure 2.2: Comparison of background brightness measured by Coihueco FD bay 4 and Solar EUV flux. Pearson correlation coefficient $r = 0.63$.

## 2.4 Analysis of the signal using the upper half of FD cameras

FD detectors look into elevations from 2° to 29°. If we consider only the signal from upper half of FD detector we may avoid potential influence due to scattered

light of human light pollution close to the horizon.

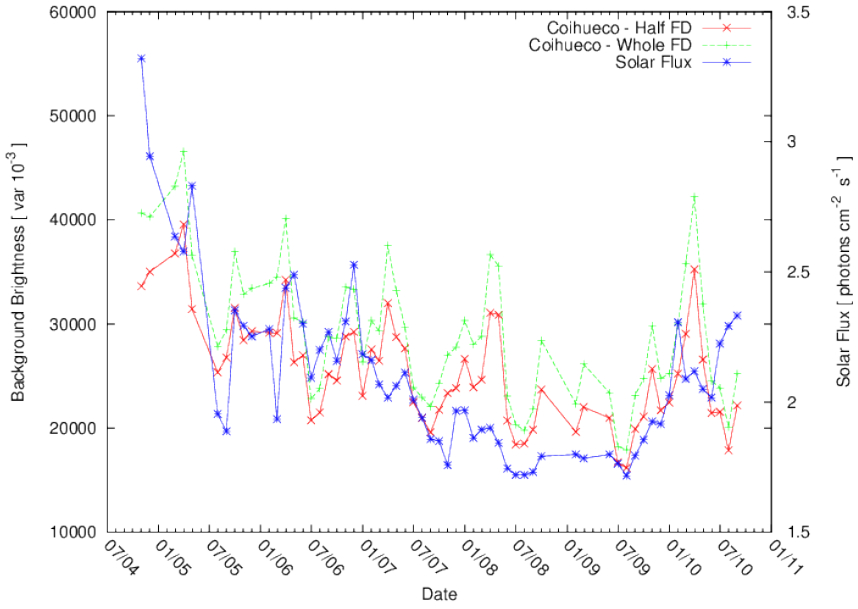


Figure 2.3: Comparison of background brightness measured by Coihueco FD bay 4 and Solar EUV flux. Pearson correlation coefficient $r = 0.65$

Data processing is the same as before. The only difference is that the the signal from lower half or photomultiplier array is excluded.

According to the Pearson correlation coefficient, it is clear that for Los Leones FD, correlation is the same or better than before.

In case of Coihueco FD station correlation is better than before except the last bay. The best correlation was achieved at the bay 4. Correlation coefficient is now equal to $r = 0.65$ that shows very good correlation. If one looks at the Figure 2.3, the deviations around May 2008 and April 2010, which were mentioned sooner, are still very strong. Since signal from upper half of FDs is included, it is clear that these deviations aren't caused by artificial light pollution. Graphs and Pearson coefficients concerning other FDs are in Attachments.

## 2.5 Exclusion of cloudy nights

To improve the correlation and eliminate discrepances, cloudy nights were excluded. At the Pierre Auger Observatory there is a system of LIDAR stations. At each FD station there is also one LIDAR station. LIDARs main purpose is to precise monitor of the atmosphere. The atmosphere acts as a calorimeter and it is necessary to know its actual state to perform appropriate calibrations of FD data.

At each LIDAR station, UV laser sends short pulses. Photomultipliers detect backscattered signal. Acquired data contain informations about atmospheric parameters in particular the information about cloud cover. LIDAR data are stored in the database.

We have tested the hypothesis that some discrepances mentioned before are the consequence of cloudiness. Cloudines was examined in case of Los Leones and

Coihueco FD stations. Los Morados FD station was excluded from this analysis because there are not enough cloud data in LIDAR database for Los Morados FD.

We have used data, where signal only from upper part of FD is included. We have selected nights when cloud cover was less than 30%. However, according to the Pearson coefficients, the correlation wasn't better than before. Except Los Leones bay 1, the correlation was worse and the discrepances which were considered as the consequence of cloudiness were still noticeable. We have expected much better correlation because we believed that the major damaging effect is due to cloudiness.

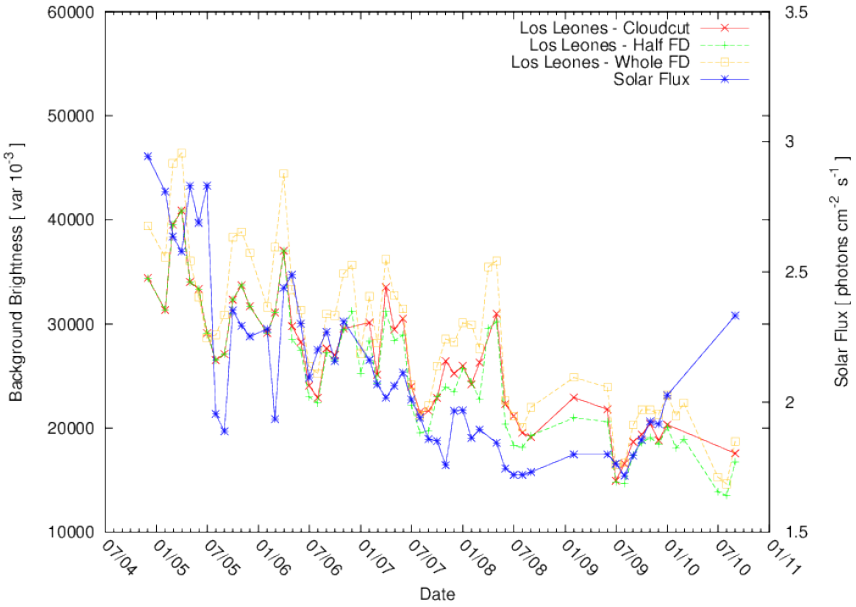


Figure 2.4: Comparison of background brightness measured by Los Leones FD bay 1 and Solar EUV flux. Pearson correlation coefficient $r = 0.71$

In case of Los Leones bay 1 the correlation coefficient is equal to $r = 0.71$. At the Figure 2.4 there is a graph of background brightness compared to solar EUV flux. On one hand it is evident that peak around May 2008 is still there on the other hand the peak around April 2010 was reduced. Unfortunately Los Leones bay 1 is the only example where this discrepance was reduced. Inspecting other bays or FD stations, the discrepance is still noticeable. So we aren't allowed to claim that these discrepances are caused by cloudiness. Other graphs and Pearson coefficients are in an Attachments.

# 3. Exclusion of the data with high level of uncertainty

Note that in chapter 2 the uncertainty of FD measurements was not mentioned at all. For proper interpretation of results it is necessary to take the fluctuations of FD measurements into account. Measurements could be biased by very high value of uncertainty. These fluctuations can be caused by changeable weather, human activities like human light pollution or by hardware error. Including such a measurements could affect data analysis negatively.

The square root of statistical dispersion is calculated for each measurement. It means that fluctuation of the background signal is computed across the 440 photomultipliers of the area at one time, thus it is computed for each frame from 440 photomultiplier variance values. It was determined that mean value of relative uncertainty, which is obtained from the square root of statistical dispersion, is approximately 15%. We denote this value $\sigma$. We took into consideration that variances with high relative uncertainty could affect analysis negatively. According to this idea the data, where the uncertainty of variance measurements are higher than $2\sigma$, are excluded. After the exclusion of the measurements with high value of relative uncertainty, the whole analysis which is described in the former Chapter was carried out again. For better understanding of the analysis there are Tables 6.3, 6.4 and 6.5 in Attachments. These tables contain numbers of measurements. These numbers illustrate how the data amount decreases due to this cuts. The results which were obtained are presented below. These results are also compared with former results.

## 3.1 Analysis of the signal from all FD cameras

Filtered data obtained from Coihueco, Los Leones and Los Morados FD stations were analyzed. Data from each bay were processed separately. Signal from all PMTs of each FD telescope is included.

Considering Coihueco FD station, the outcome is approximately the same as in Section 2.3. Pearson correlation coefficients differ only in the order of few hundredths, which is negligible difference.

The same results were obtained in case of Los Leones except Los Leones bay 6, where the correlation has improved very much. New Pearson correlation coefficient is equal to $r_{2\sigma} = 0.73$ whereas the old one is equal to $r = 0.56$. At the Figure 3.1 there is a graph of background brightness measured by Los Leones bay 6 compared to solar EUV flux.

Assuming Los Morados FD station there is also only negligible difference between the correlation coefficients quoted in Section 2.3 and new ones.

At the Figure 3.1 one can notice that the deviance around May 2008 is still quite strong. Unfortunately in case of Los Leones bay 6, data since the beginning of 2009 were not available. In the Attachments, there are graphs considering other bays and it is evident, that also the deviance around April 2010 was not reduced.

All Pearson coefficients concerning other bays are given in Attachments.

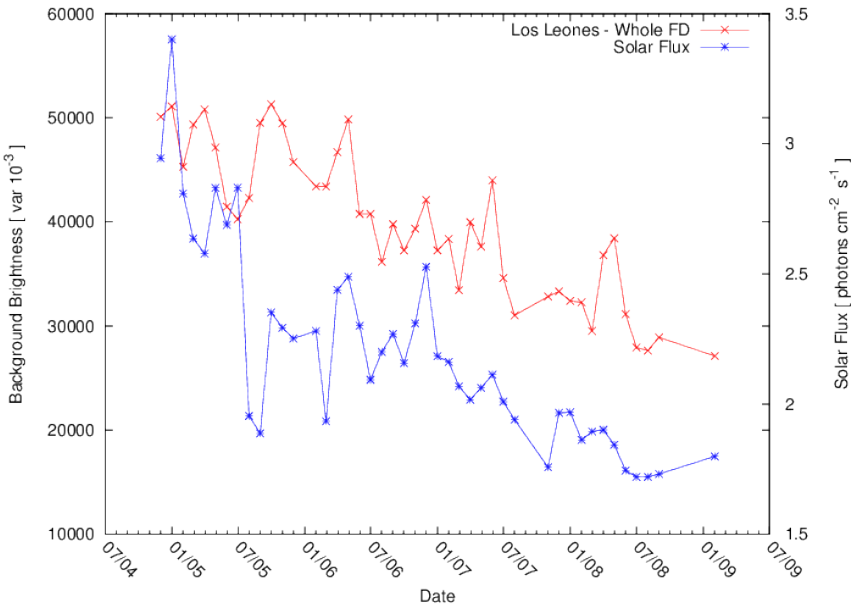


Figure 3.1: Comparison of background brightness measured by Los Leones FD bay 6 and Solar EUV flux. Pearson correlation coefficient $r = 0.73$.

## 3.2 Analysis of the signal from upper half of FD cameras

Again the filtered data were used for this analysis. As it was described in Section 2.4 we excluded the signal from lower half of photomultiplier array due to the negative influence of human light pollution close to the horizon.

Considering Coihueco and Los Morados FD stations, Pearson coefficients gained from filtered data are approximately the same as coefficients gained from unfiltered data. There are only some negligible differences.

In case of Los Leones FD, only one significant difference is apparent. New Pearson coefficient for Los Leones bay 6 is equal to $r_{2\sigma} = 0.70$ whereas the old one is equal to $r = 0.56$. Time development of background brightness measured by Los Leones bay 6 together with solar EUV flux is at the Figure 3.2. The deviance around May 2008 is apparently the same as in case of whole FD analysis.

All Figures and Pearson coefficients concerning other bays and FDs are quoted in Attachments. When one compares the result of whole FD analysis and half FD analysis there are no significant differences in the time development trend.

## 3.3 Exclusion of cloudy nights

The analysis was carried out in the same way as it was described in Section 2.5. In comparision to the results presented in Section 2.5, the correlation got worse. For example new Pearson coefficient for Los Leones bay 1 is now equal to $r_{2\sigma} = 0.62$ whereas the old one was equal to $r = 0.71$ Time development of background brightness measured by Los Leones bay 1 together with solar EUV flux is at the Figure 3.3.

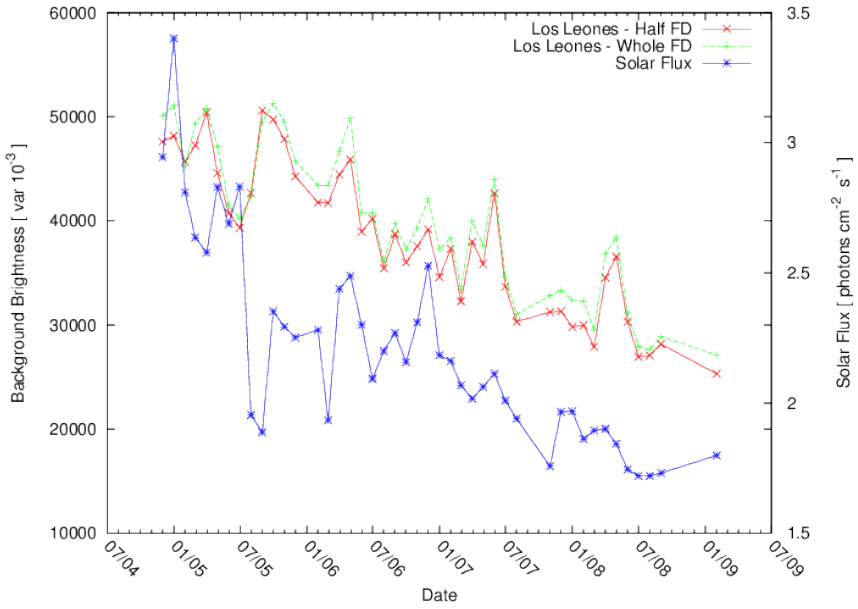


Figure 3.2: Comparison of background brightness measured by Los Leones FD bay 6 and Solar EUV flux. Pearson correlation coefficient $r = 0.70$.

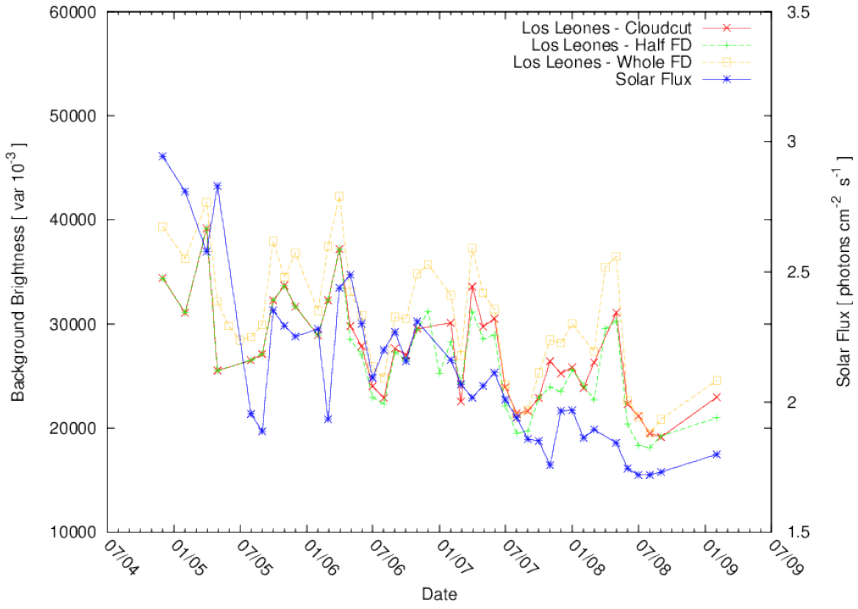


Figure 3.3: Comparison of background brightness measured by Los Leones FD bay 1 and Solar EUV flux. Pearson correlation coefficient $r = 0.62$.

# 4. Anomalies

In Chapter 2 were mentioned some anomalies, which are noticeable in all FDs. These deviances aren't possibly related to ordinary atmospheric events. Each point in the graph is related to one month in the year so it is unlikely that some short time event is the cause of these deviances. We can exclude lightings and other rare atmospheric effects. The date of occurrence of the first deviance is very close to the big eruption of volcano Chaitén which erupted on 2$^{nd}$ May 2008. It is possible that small-grained dust and ash caused that more light was scattered. This increase of background brightness was registered by all FDs.

Although the second anomaly is very close to the eruption of Eyjafjallajökull volcano which erupted on the 20$^{th}$ March 2010 and 14$^{th}$ April 2010 again, it is very unlikely that this eruption affected night sky brightness in South America. First and second anomaly is labeled in the Figure 4.1.

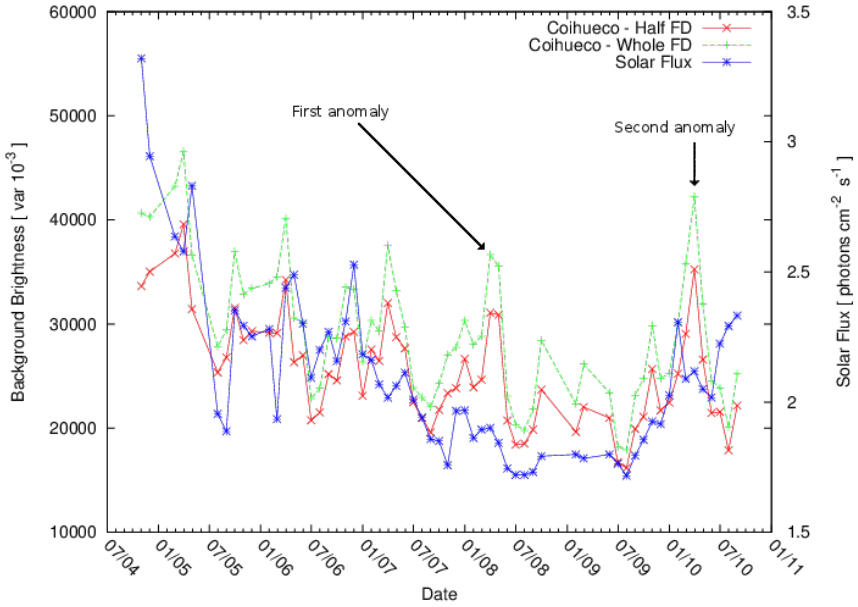


Figure 4.1: First and second anomaly as was measured by Coihueco 4.

In Chapter 3 we also discussed these deviances. We expected that the removal of the data which are biased by a large uncertainty might reduce these deviances. It turned out that the deviances didn't changed at all. According this fact we can claim that the first anomaly is quite likely caused by the eruption of Chaitén volcano and the data biased by high level of uncertainty aren't the source of the deviances.

We assumed that the impact of Eyjafjallajökull volcano eruption on the night sky brightness is very low so the second anomaly is most likely not caused by the eruption of this volcano. As we know, there was no extraordinary event which could intensely affect night sky brightness in South America around April 2010. We have to conclude that the source of this anomaly is unknown for now.

The last anomaly is noticeable at the plot of Los Leones bay 6. This plot is at the Figure 4.2. It is obvious that after June 2009 the values of background

brightness variances systematically decreased. Several photomultipliers were removed and they were used for HEAT telescope. This removal was done at Los Leones 6 intentionally. The field of view of Los Leones 6 is affected by human light pollution from Malargüe town. In spite of this fact, we still handle these data like there is full number of photomultipliers. While the mean value of variances is calculated, the former number of photomultipliers is used and it because we obtain systematically lower mean value.

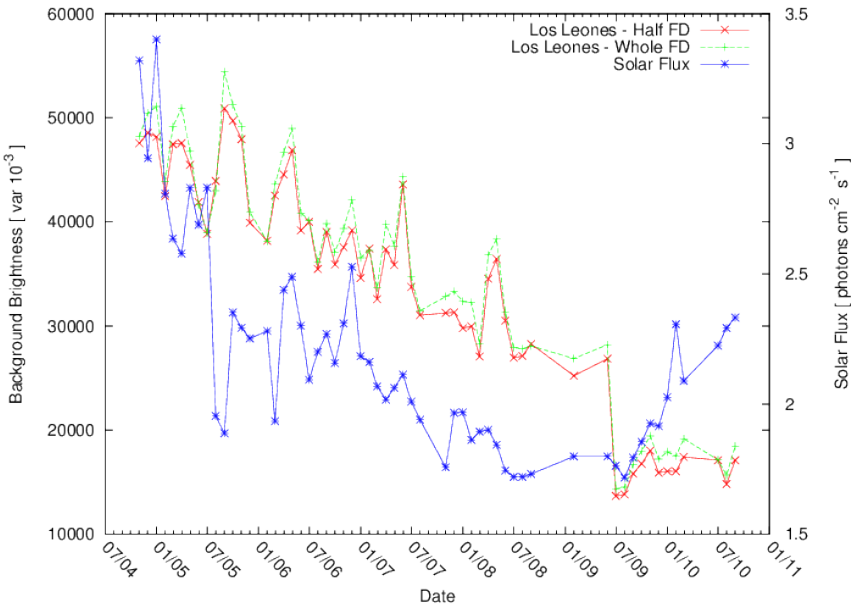


Figure 4.2: Systematicly lower value of variances is clearly noticeable at Los Leones bay 6.

# 5. Discussion

Night sky brightness and solar EUV flux were compared on the long time scale. Comparison was made several times with a few modifications. The significance of the correlation was determined by Pearson correlation coefficient.

In first case comparison was made in the simplest way. Signal from whole surface of FD detector was included into the analysis. Considering Los Leones and Coihueco FD stations correlation was quite high according to the Pearson correlation coefficient. In case of Los Morados FD station, Pearson correlation coefficients were systematically lower. The cause of much worse correlation in case of Los Morados FD could lie in the azimuthal direction of its field of view. The field of view of Los Morados bays contains mostly the area above the Andes. It is possible that some specific atmospheric events like cloudiness above mountains or storms, which are common in the mountain area, influence background brightness of the sky above the Andes.

For better comparison of background brightness measured by all bays of each FD one can look at Figures 5.1, 5.2 and 5.3. We used the data, where signal from upper half of FD is included.

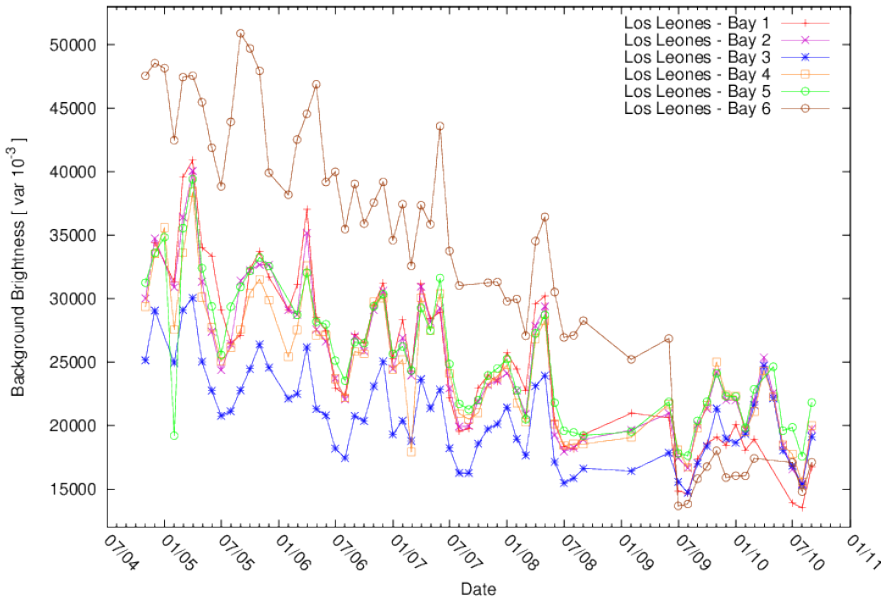


Figure 5.1: Comparison of background brightness measured by all bays of Los Leones FD.

Anyway there are some deviances which were measured by all FDs. First attempt to eliminate these deviances was neglecting the signal from lower part of FD to eliminate impact of human light pollution. After this was applied, correlation was better but the strong deviances mentioned before were still noticeable. However in case of Los Leones 6 there is still noticeable strong influence of human light pollution caused by Malargüe town as one can see at the Figure 5.1. The values of variance is obviously higher than in case of other bays.

Next attempt to make correlation better was excluding the data affected by cloudiness. If cloudiness covered more than 30% of the sky FD measurements were

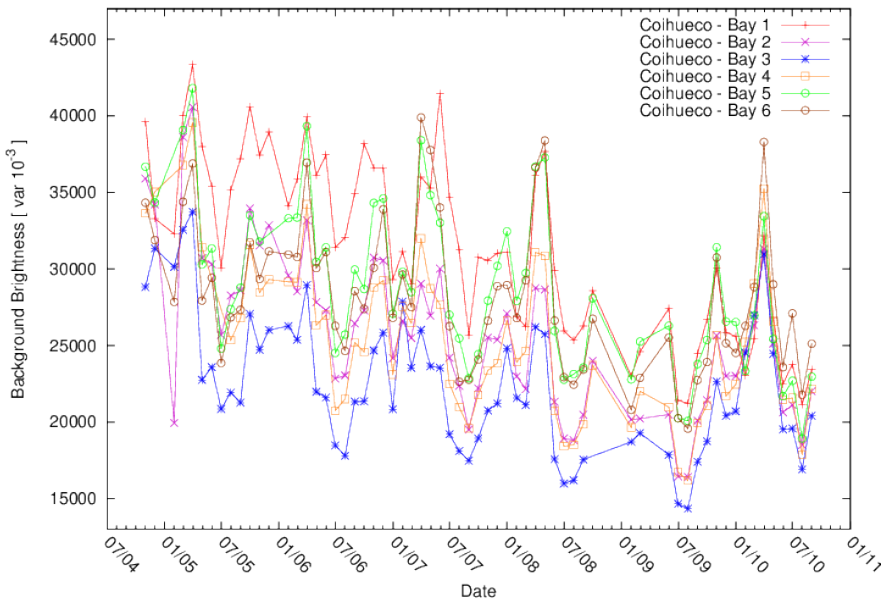


Figure 5.2: Comparison of background brightness measured by all bays of Coihueco FD.

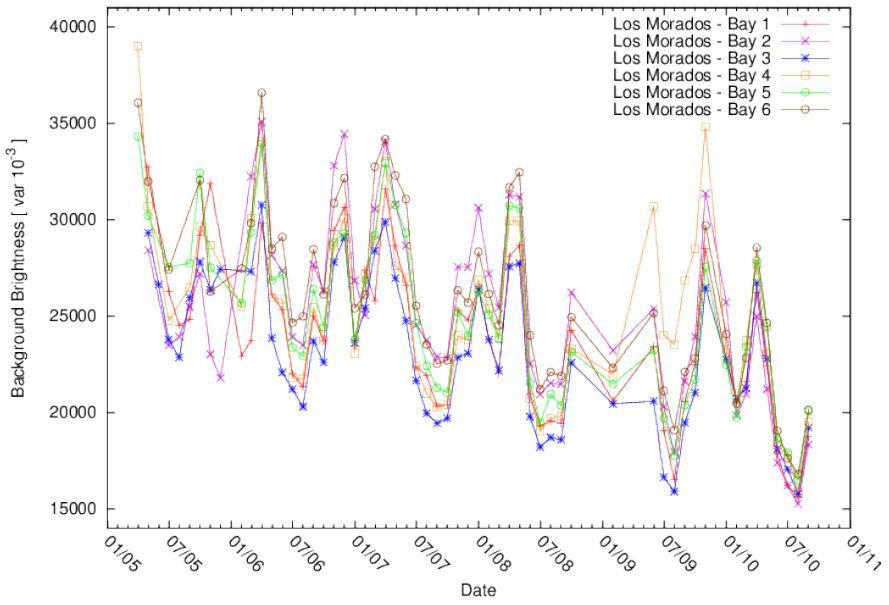


Figure 5.3: Comparison of background brightness measured by all bays of Los Morados FD.

excluded. Correlation coefficients decreased and according the graphs strong deviances are still there.

The last attempt to improve analysis and inspecting the source of anomalies was exclusion of the data biased by high level of uncertainty. It is evident that none of the deviance was reduced. It is confirming us that the deviances are of natural origin, in other words it is not the consequence of poor-quality data.

The impact on the correlation coefficients was various. The correlation didn't changed significantly in most cases but there are a few of examples where the correlation was higher and also some instances of lowering. We expect that the

lowering is related to the reduced amount of data.

Assuming these results, it is certain that human light pollution was affecting the comparison and excluding the lower part of FDs improved the correlation, however it has no impact on some deviances which are noticeable in the graphs. It is quite possible that these deviances are caused by some rare events like volcano eruption. This alternative was discussed in Chapter 4.

# Conclusion

We can claim that in case of all FDs correlation was quite high according to Pearson correlation coefficients, moreover there are some periods when time development of background brightness was very similar to solar EUV flux time development. On the basis of theoretical preconditions it was proved that night sky brightness correlates with solar cycle. We should emphasize that this is the first time when the correlation was proved using the background data measured by fluorescence telescopes. It is clear that there is no possibility to reach Pearson correlation coefficient which would be approaching to $r = 1$ because other factors influence the background brightness and there is no possibility to include the influence of these factors into the analysis.

# Bibliography


[1] Benn, Chris - Ellison, Sara. Brightness of the Night Sky Over La Palma. *New Astronomy Reviews,* November 1998, vol. 42, issues 6 - 8, p. 504 - 507.

[2] Caruso, Rossella - Petrera, Sergio. Measurement of the Sky Photon Background Flux at Los Leones. *$29^{th}$ International Cosmic Ray Conference Pune,* August 2005.

[3] *CELIAS/SEM experiment on the Solar Heliospheric Observatory data.* URL: <http://www.usc.edu/dept/space_science/sem_data/sem_data.html> [cited 2011-09-01]

[4] Stanev, Todor. *High Energy Cosmic Rays.* Second Edition, 2010. Chichester: Springer. ISBN 978-3-540-85147-9

[5] Allekotte, Ingo et al. The surface detector system of the Pierre Auger Observatory. *Nuclear Instruments and Methods in Physics Research Section A: Accelerators, Spectrometers, Detectors and Associated Equipment,* March 2008, vol. 586, issue 3, p. 409 - 420.

[6] Arqueros, Fernando - Hörandler, Jörg - Keilhauer, Bianca. Air fluorescence relevant for cosmic-ray detection - Summary of the 5th fluorescence workshop, El Escorial 2007. *Nuclear Instruments and Methods in Physics Research Section A: Accelerators, Spectrometers, Detectors and Associated Equipment,* November 2008, vol. 597, issue 1, p. 1 - 22.

[7] Barth, Charles - Kaplan, Joseph. Herzberg Oxygen Bands in "Air" Afterglows and the Night Airglow *The Journal of Chemical Physics,* March 1957, vol. 26, issue 3, p. 506 - 510.

[8] Pierre Auger Collaboration. The Fluorescence Detector of the Pierre Auger Observatory *Nuclear Instruments and Methods in Physics Research Section A: Accelerators, Spectrometers, Detectors and Associated Equipment,* August 2010, vol. 620, issues 2 - 3, p. 227 - 251.

[9] Rodgers, Joseph - Nicewander, Alan. Thirteen Ways to Look at the Correlation Coefficient *The American Statistician,* February 1988, vol. 43, issue 1, p. 59 - 66.

[10] Prouza, Michael. Doctoral Thesis: *Ultra-High Energy Cosmic Rays and Theirs Detection in Auger Project.* Prague 2005.

[11] Cohen, Jacob. *Statistical Power Analysis for the Behavioral Sciences* Second Edition, 1988. Lawrence Erlbaum Associates, ISBN 0-8058-0283-5

# List of Tables

# Attachments

## Tables

| Bay | Los Leones | Coihueco | Los Morados |
|---|---|---|---|
| **1** | 29.8.2005 | 1.9.2005 | 10.11.2005 |
| **2** | 26.8.2005 | 2.2.2005 | 16.11.2005 |
| **3** | 1.7.2004 | 1.2.2004 | 27.8.2005 |
| **4** | 1.4.2003 | 31.7.2004 | 1.6.2005 |
| **5** | 2.2.2005 | 16.1.2006 | 1.6.2005 |
| **6** | 29.8.2005 | 16.1.2006 | 27.8.2005 |

Table 6.1: Correction rings instalation dates

| | **Whole FD** | | **Half FD** | | **Cloud cut** | |
|---|---|---|---|---|---|---|
| | $\sigma < 100\%$ | $\sigma < 30\%$ | $\sigma < 100\%$ | $\sigma < 30\%$ | $\sigma < 100\%$ | $\sigma < 30\%$ |
| **Coihueco 1** | 0.49 | 0.50 | 0.49 | 0.53 | 0.38 | 0.43 |
| **Coihueco 2** | 0.60 | 0.60 | 0.62 | 0.62 | 0.55 | 0.54 |
| **Coihueco 3** | 0.60 | 0.56 | 0.61 | 0.58 | 0.55 | 0.52 |
| **Coihueco 4** | 0.65 | 0.63 | 0.66 | 0.65 | 0.61 | 0.61 |
| **Coihueco 5** | 0.45 | 0.46 | 0.46 | 0.46 | 0.36 | 0.36 |
| **Coihueco 6** | 0.40 | 0.39 | 0.39 | 0.38 | 0.24 | 0.22 |
| **Los Leones 1** | 0.56 | 0.57 | 0.63 | 0.66 | 0.71 | 0.62 |
| **Los Leones 2** | 0.59 | 0.61 | 0.59 | 0.59 | 0.59 | 0.59 |
| **Los Leones 3** | 0.65 | 0.65 | 0.66 | 0.65 | 0.66 | 0.65 |
| **Los Leones 4** | 0.63 | 0.63 | 0.64 | 0.65 | 0.64 | 0.65 |
| **Los Leones 5** | 0.59 | 0.56 | 0.59 | 0.56 | 0.59 | 0.54 |
| **Los Leones 6** | 0.56 | 0.73 | 0.56 | 0.70 | 0.60 | 0.68 |
| **Los Morados 1** | 0.39 | 0.44 | 0.43 | 0.42 | — | — |
| **Los Morados 2** | 0.18 | 0.22 | 0.17 | 0.16 | — | — |
| **Los Morados 3** | 0.44 | 0.43 | 0.43 | 0.43 | — | — |
| **Los Morados 4** | 0.30 | 0.35 | 0.29 | 0.31 | — | — |
| **Los Morados 5** | 0.45 | 0.42 | 0.44 | 0.47 | — | — |
| **Los Morados 6** | 0.40 | — | 0.40 | — | — | — |

Table 6.2: Pearson correlation coefficients achieved with different analysis methods

In Tables 6.3, 6.4 and 6.5 there are numbers of measurements and numbers of gained medians or mean values. *Filter 1* accepts only data with variances higher than 10 and lower than 100. *Days after filter 1* is number of daily medians gained from the data which were accepted by *Filter 1*. *Filter 2* accepts only such a days when more than 400 measurements were used for calculating daily median. *Months after filter 2* is the number of monthly averages gained from filtered daily median. Monthly average is quantified only if there are 5 or more daily medians available.

| | **Number of measurements** | **Measeurements after filter 1** | **Days after filter 1** | **Days after filter 2** | **Months after filter 2** |
|---|---|---|---|---|---|
| **Coihueco 1** | 654749 | 622019 | 947 | 703 | 62 |
| **Coihueco 2** | 658433 | 615114 | 540 | 640 | 58 |
| **Coihueco 3** | 651767 | 551699 | 912 | 592 | 55 |
| **Coihueco 4** | 644190 | 583040 | 922 | 639 | 58 |
| **Coihueco 5** | 655344 | 613716 | 943 | 692 | 60 |
| **Coihueco 6** | 651613 | 617539 | 940 | 699 | 64 |
| **Los Leones 1** | 769839 | 536509 | 814 | 492 | 42 |
| **Los Leones 2** | 806874 | 740333 | 952 | 673 | 61 |
| **Los Leones 3** | 817245 | 772437 | 957 | 723 | 62 |
| **Los Leones 4** | 816199 | 789463 | 961 | 737 | 63 |
| **Los Leones 5** | 805524 | 776603 | 928 | 723 | 60 |
| **Los Leones 6** | 755671 | 498404 | 695 | 492 | 44 |
| **Los Morados 1** | 602863 | 497836 | 822 | 585 | 52 |
| **Los Morados 2** | 600760 | 516789 | 854 | 594 | 53 |
| **Los Morados 3** | 617140 | 534989 | 848 | 626 | 55 |
| **Los Morados 4** | 608762 | 502805 | 846 | 589 | 52 |
| **Los Morados 5** | 605294 | 405676 | 840 | 511 | 54 |
| **Los Morados 6** | 606659 | 67224 | 362 | 51 | 3 |

Table 6.3: Numbers of data for analysis of the signal from all FD cameras.

| | Number of measurements | Measeurements after filter 1 | Days after filter 1 | Days after filter 2 | Months after filter 2 |
|---|---|---|---|---|---|
| **Coihueco 1** | 654749 | 607036 | 941 | 702 | 62 |
| **Coihueco 2** | 658433 | 604576 | 935 | 701 | 63 |
| **Coihueco 3** | 651767 | 562101 | 895 | 641 | 58 |
| **Coihueco 4** | 644190 | 579651 | 918 | 677 | 61 |
| **Coihueco 5** | 655344 | 623099 | 941 | 717 | 62 |
| **Coihueco 6** | 651613 | 612262 | 938 | 697 | 64 |
| **Los Leones 1** | 769839 | 473164 | 716 | 511 | 42 |
| **Los Leones 2** | 806874 | 744912 | 942 | 715 | 62 |
| **Los Leones 3** | 817245 | 755342 | 947 | 724 | 62 |
| **Los Leones 4** | 816199 | 764395 | 961 | 715 | 62 |
| **Los Leones 5** | 805524 | 768380 | 928 | 724 | 60 |
| **Los Leones 6** | 755671 | 463974 | 679 | 486 | 44 |
| **Los Morados 1** | 602863 | 534770 | 822 | 611 | 53 |
| **Los Morados 2** | 600760 | 543055 | 850 | 631 | 55 |
| **Los Morados 3** | 617140 | 569834 | 848 | 654 | 56 |
| **Los Morados 4** | 608762 | 549996 | 850 | 625 | 54 |
| **Los Morados 5** | 605294 | 489370 | 841 | 586 | 54 |
| **Los Morados 6** | 606659 | 56023 | 151 | 69 | 6 |

Table 6.4: Numbers of data for analysis of the signal from upper half of FD cameras.

| | Number of measurements | Measeurements after filter 1 | Days after filter 1 | Days after filter 2 | Months after filter 2 |
|---|---|---|---|---|---|
| **Coihueco 1** | 451349 | 415576 | 842 | 477 | 52 |
| **Coihueco 2** | 456676 | 416594 | 837 | 481 | 52 |
| **Coihueco 3** | 449080 | 379032 | 793 | 430 | 48 |
| **Coihueco 4** | 441640 | 392320 | 819 | 455 | 50 |
| **Coihueco 5** | 453076 | 428840 | 845 | 493 | 53 |
| **Coihueco 6** | 450187 | 420548 | 836 | 481 | 52 |
| **Los Leones 1** | 530223 | 339240 | 654 | 368 | 39 |
| **Los Leones 2** | 555462 | 515257 | 846 | 520 | 57 |
| **Los Leones 3** | 564734 | 526957 | 848 | 524 | 57 |
| **Los Leones 4** | 563767 | 523009 | 864 | 510 | 56 |
| **Los Leones 5** | 556526 | 525660 | 835 | 525 | 54 |
| **Los Leones 6** | 527902 | 349525 | 624 | 363 | 38 |

Table 6.5: Numbers of data for analysis with exclusion of cloudy nights.

# Analysis with no cut on high level of uncertainty

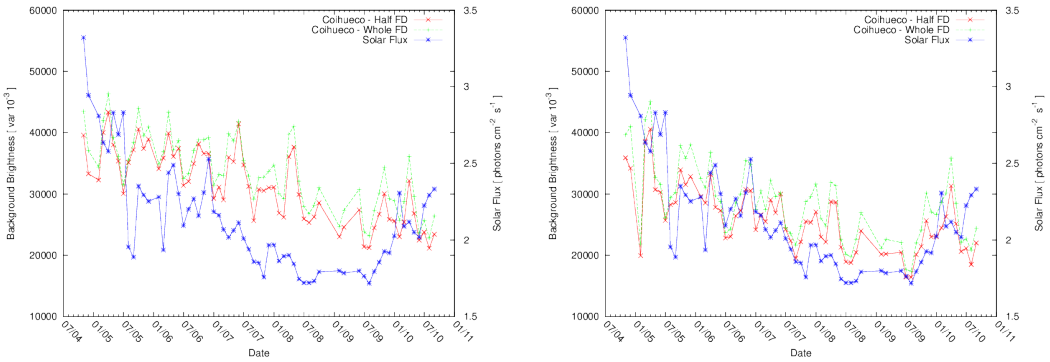


Figure 6.1: Coihueco bay 1 and Coihueco bay 2

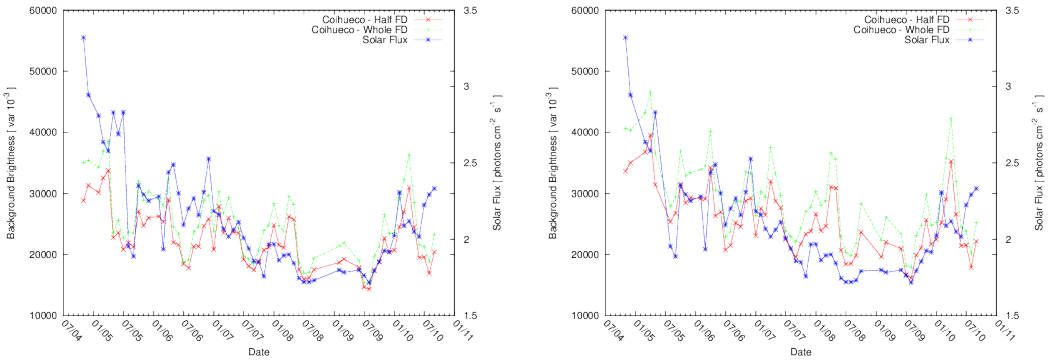


Figure 6.2: Coihueco bay 3 and Coihueco bay 4

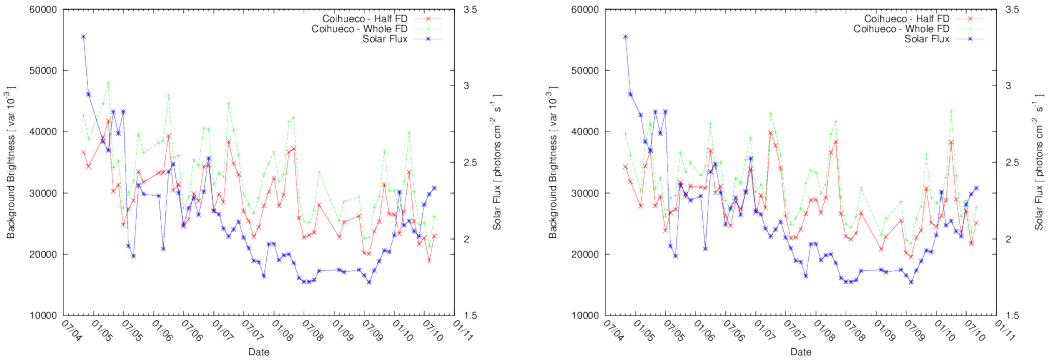


Figure 6.3: Coihueco bay 5 and Coihueco bay 6

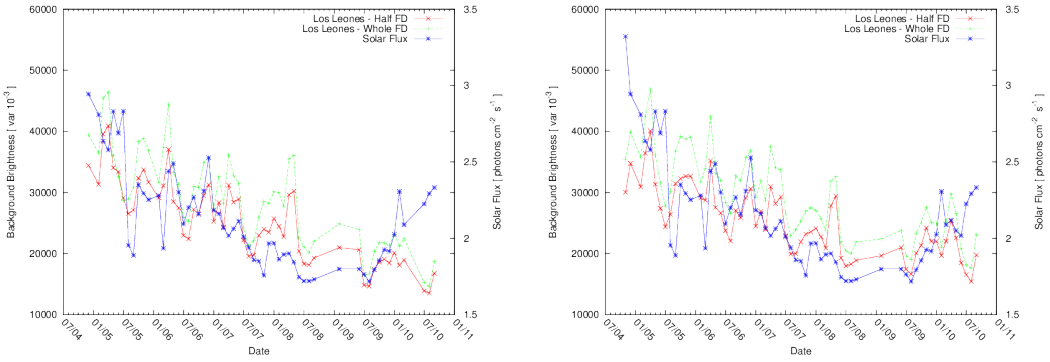


Figure 6.4: Los Leones bay 1 and Los Leones bay 2

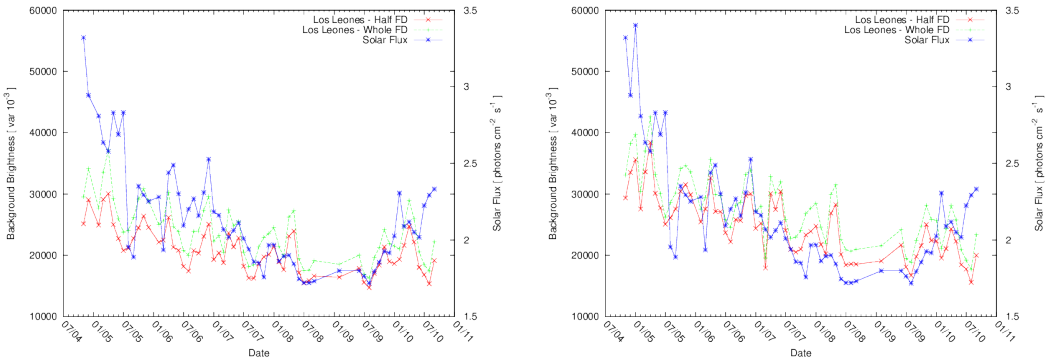


Figure 6.5: Los Leones bay 3 and Los Leones bay 4

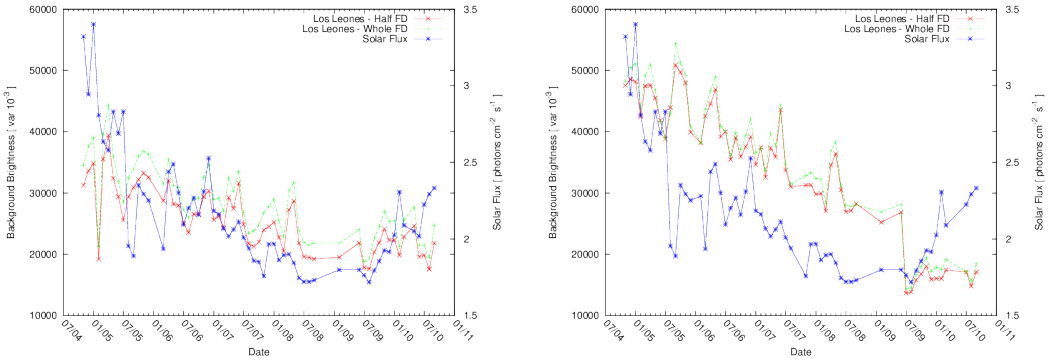


Figure 6.6: Los Leones bay 5 and Los Leones bay 6

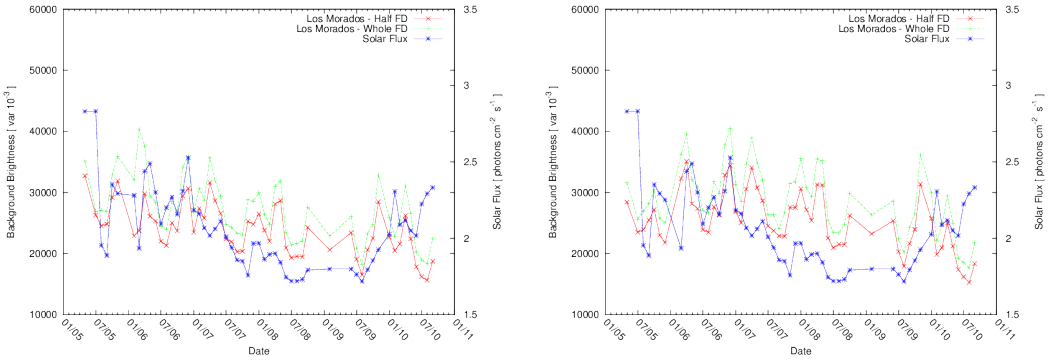


Figure 6.7: Los Morados bay 1 and Los Morados bay 2

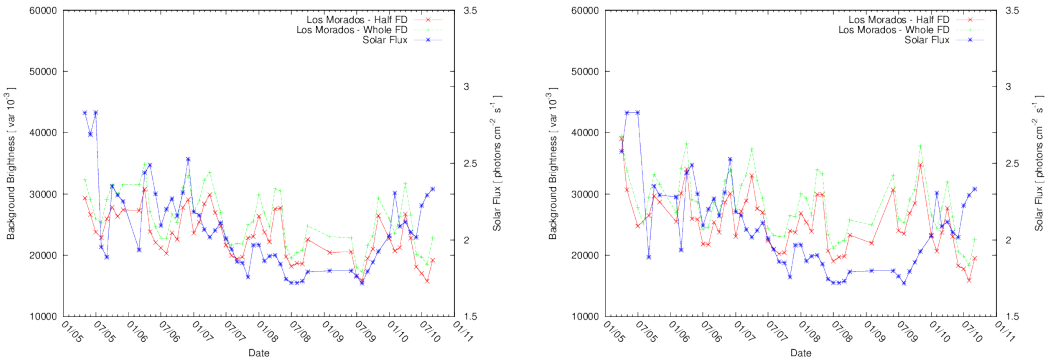


Figure 6.8: Los Morados bay 3 and Los Morados bay 4

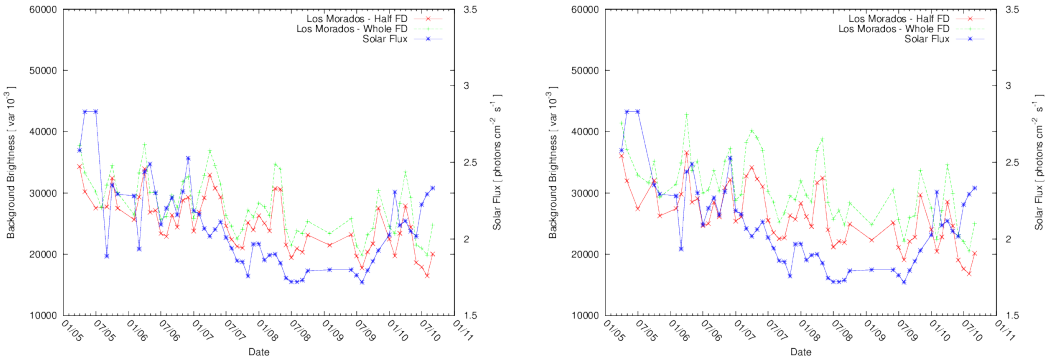


Figure 6.9: Los Morados bay 5 and Los Morados bay 6

# Analysis with $2\sigma$ cut on high level of uncertainty

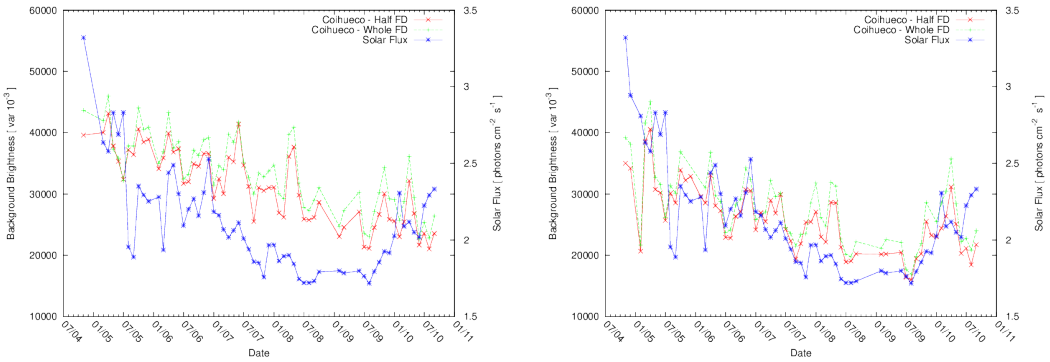


Figure 6.10: Coihueco bay 1 and Coihueco bay 2

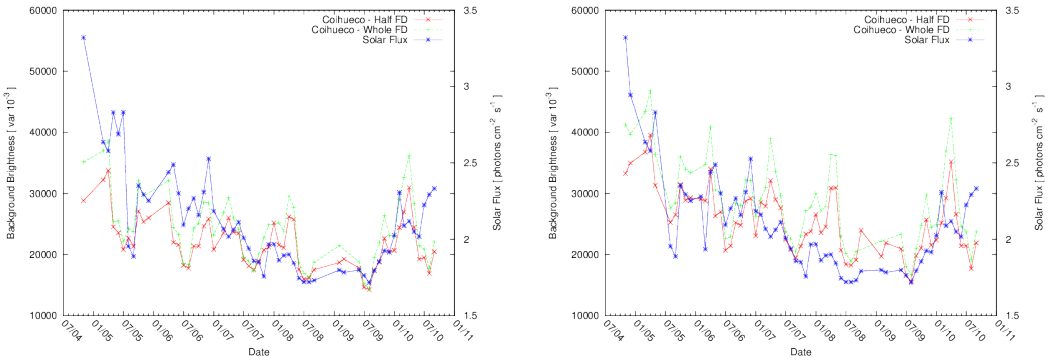


Figure 6.11: Coihueco bay 3 and Coihueco bay 4

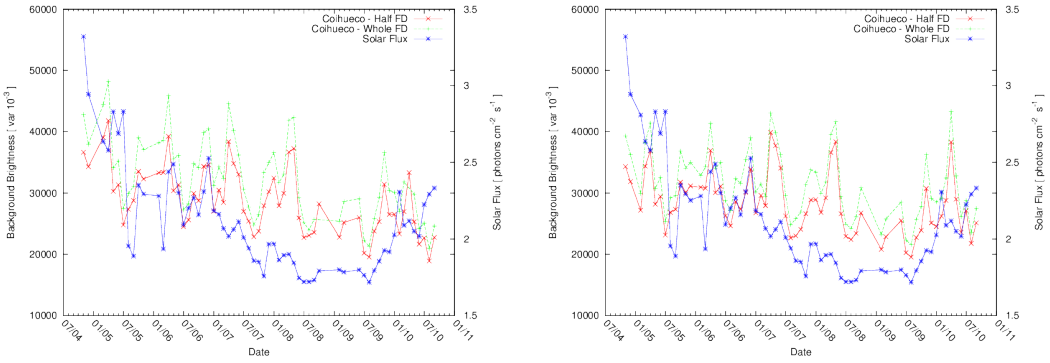


Figure 6.12: Coihueco bay 5 and Coihueco bay 6

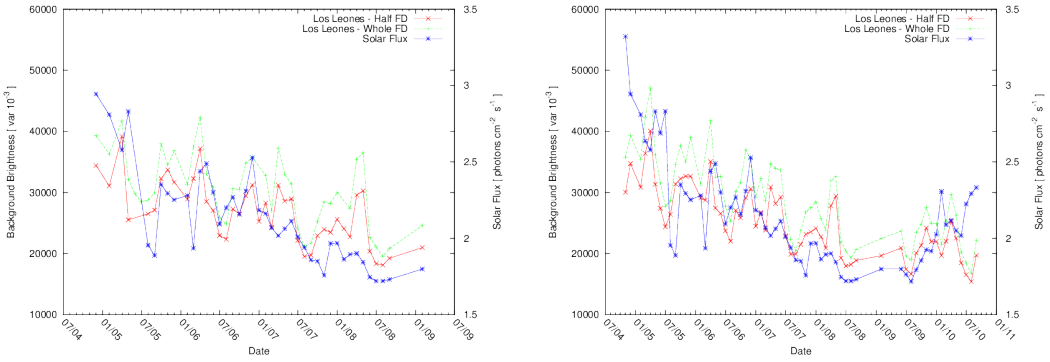


Figure 6.13: Los Leones bay 1 and Los Leones bay 2

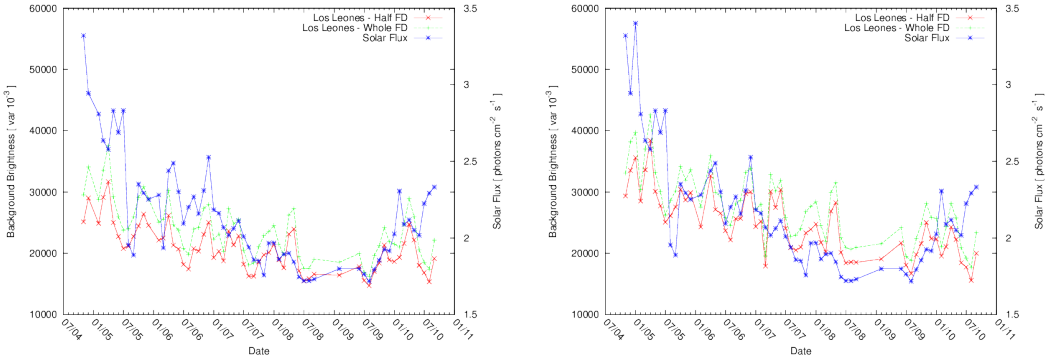


Figure 6.14: Los Leones bay 3 and Los Leones bay 4

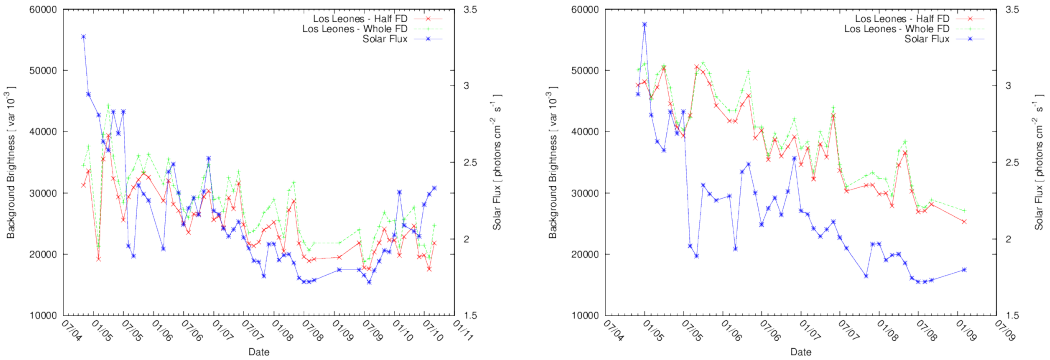


Figure 6.15: Los Leones bay 5 and Los Leones bay 6

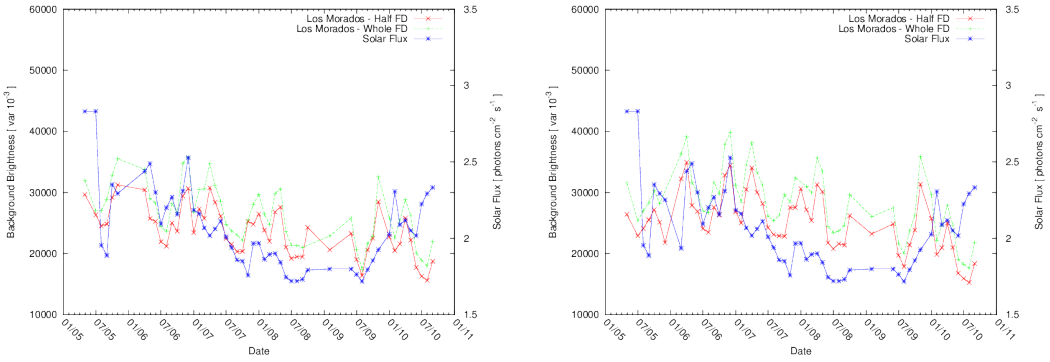


Figure 6.16: Los Morados bay 1 and Los Morados bay 2

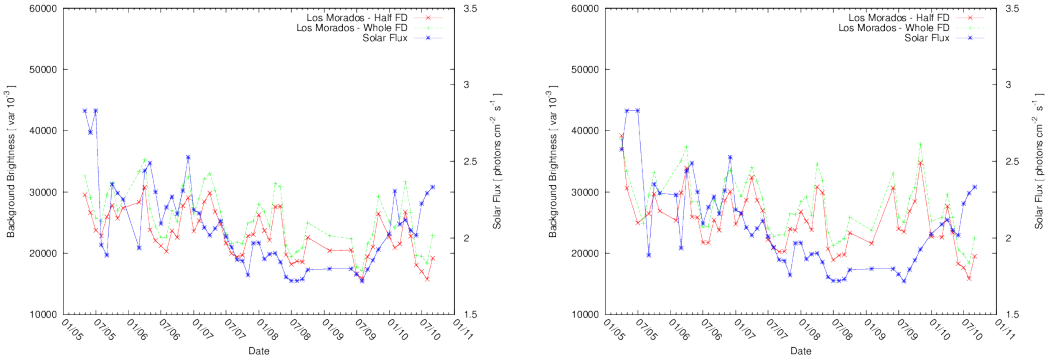


Figure 6.17: Los Morados bay 3 and Los Morados bay 4

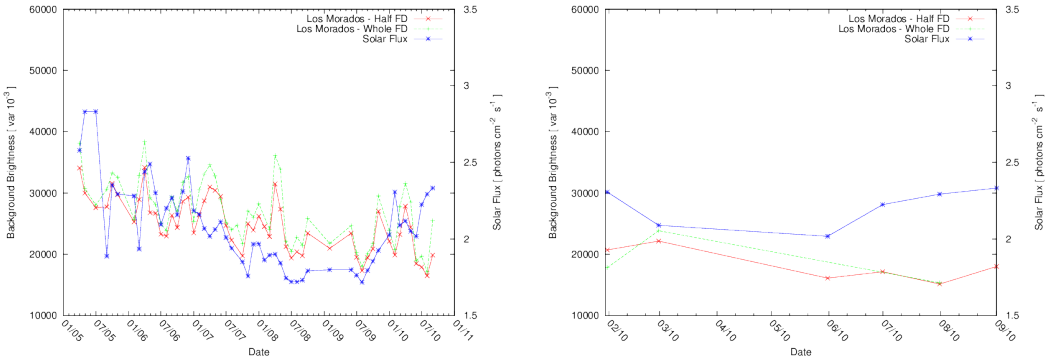


Figure 6.18: Los Morados bay 5 and Los Morados bay 6